

Identifying the Orientation of Edge of Graphene Using G band Raman Spectra

Ken-ichi SASAKI¹ *, Riichiro SAITO², Katsunori WAKABAYASHI^{1,3}, and Toshiaki ENOKI⁴

¹ *International Center for Materials Nanoarchitectonics,*

National Institute for Materials Science, Namiki, Tsukuba 305-0044, Japan

² *Department of Physics, Tohoku University, Sendai 980-8578, Japan*

³ *PRESTO, Japan Science and Technology Agency, Kawaguchi 332-0012, Japan*

⁴ *Department of Chemistry, Tokyo Institute of Technology, Ookayama, Meguro-ku, Tokyo 152-8551, Japan*

(Received June 23, 2018)

The electron-phonon matrix elements relevant to the Raman intensity and Kohn anomaly of the G band are calculated by taking into account the effect of the edge of graphene. The analysis of the pseudospin reveals that the longitudinal optical phonon mode undergoes a strong Kohn anomaly for both the armchair and zigzag edges, and that only the longitudinal (transverse) optical phonon mode is a Raman active mode near the armchair (zigzag) edge. The Raman intensity is enhanced when the polarization of the incident laser light is parallel (perpendicular) to the armchair (zigzag) edge. This asymmetry between the armchair and zigzag edges is useful in identifying the orientation of the edge of graphene.

KEYWORDS: graphene, edge orientation, Raman spectroscopy, electron-phonon interaction, electron-light interaction, pseudospin, gauge field

1. Introduction

Graphene is a unique material since its electron motion is governed by a special equation similar to the relativistic massless Dirac equation, while a nonrelativistic equation is common in condensed matter physics.^{1,2} The electron motion is modified by the electron-phonon (el-ph) and electron-light interactions, which are fundamental issues in discussing the transport,^{1,2} electronic,³ and optical properties^{4,5} of graphene. The goal of this paper is to show that an asymmetry of the Raman spectra for Γ point longitudinal and transverse optical phonon (LO and TO) modes, both of which are known as the Raman G band, appears near the edge of graphene. There are two fundamental orientations for the edge of graphene, zigzag and armchair edges, and a general edge shape is considered to be a mixture of them.^{6,7} The asymmetry is useful in identifying the orientation of the edge of graphene by Raman spectroscopy.

In Raman spectroscopy, we irradiate laser light onto a sample and observe the intensity of the inelastically scattered light. The energy difference between the incident laser and the inelastically scattered light corresponds to the energy of a Raman active phonon mode due to the energy conservation. The el-ph interaction is essential for the Raman process. Further, the el-ph interaction can modify the energy and life-time of the phonon mode, which is known as the Kohn anomaly.⁸ Evidence for Kohn anomalies is found in the phonon dispersion of carbon nanotube,⁹ graphene,^{10,11} and graphite.¹² By examining the Kohn anomaly for the G band of carbon nanotube,¹³ a feature of the el-ph interaction such as the chirality dependence of the el-ph interaction upon the Kohn anomaly has been clarified.¹⁴ In this paper, we calculate the el-ph matrix elements relevant to the Raman intensity and Kohn anomaly of the G band of graphene within effective-mass approximation by includ-

ing the effects of the edge of graphene and polarization direction of an incident laser (and a scattered) light.

This paper is organized as follows. In § 2, we show the Hamiltonian including the el-ph interaction with respect to the Γ point optical phonon modes and the electron-light interaction. In § 3 and § 4, we calculate the matrix elements for the el-ph and electron-light interactions by taking into account of the presence of the zigzag and armchair edges, respectively. The self-energy of the LO mode is estimated in § 5 and the phonon self-energy for general edge shape is discussed. Finally, we propose two models representing the electronic states at the interior of a graphene sample and calculate the self-energies for those models in § 6. In § 7, we discuss the relationship between our result and experimental results, and summarize the results.

2. Hamiltonian

Let $\Psi_{\mathbf{K}}(\mathbf{r})$ [$\Psi_{\mathbf{K}'}(\mathbf{r})$] be the wave function for an electron near the K [\mathbf{K}'] point, the energy eigen equation for an electron near the Fermi energy of graphene is written as

$$\hat{H} \begin{pmatrix} \Psi_{\mathbf{K}}(\mathbf{r}) \\ \Psi_{\mathbf{K}'}(\mathbf{r}) \end{pmatrix} = E \begin{pmatrix} \Psi_{\mathbf{K}}(\mathbf{r}) \\ \Psi_{\mathbf{K}'}(\mathbf{r}) \end{pmatrix}. \quad (1)$$

The wave function $\Psi_{\mathbf{K}}(\mathbf{r})$ [$\Psi_{\mathbf{K}'}(\mathbf{r})$] is two-component structure, which results from that the hexagonal unit cell contains two carbon atoms [A atom (\bullet) and B atom (\circ) in Fig. 1]. The total Hamiltonian \hat{H} including the el-ph interaction with respect to the Γ point LO and TO modes, and the electron-light interaction is given by¹⁵

$$\hat{H} = v_{\text{F}} \begin{pmatrix} \boldsymbol{\sigma} \cdot (\hat{\mathbf{p}} + \mathbf{A}^{\text{q}} - e\mathbf{A}) & 0 \\ 0 & \boldsymbol{\sigma}' \cdot (\hat{\mathbf{p}} - \mathbf{A}^{\text{q}} - e\mathbf{A}) \end{pmatrix}. \quad (2)$$

Here v_{F} is the Fermi velocity, momentum operator $\hat{\mathbf{p}} = -i\hbar(\partial_x, \partial_y)$, $\boldsymbol{\sigma} \equiv (\sigma_x, \sigma_y)$ and $\boldsymbol{\sigma}' \equiv (-\sigma_x, \sigma_y)$ where σ_x , σ_y and σ_z are Pauli matrices. We take x and y axes as shown by the inset in Fig. 1(a). The electromagnetic

*E-mail address: SASAKI.Kenichi@nims.go.jp

gauge field \mathbf{A} enters into the Hamiltonian through the substitution $\hat{\mathbf{p}} \rightarrow \hat{\mathbf{p}} - e\mathbf{A}$ where $-e$ is the charge of electron. A uniform field \mathbf{A} can represent the incident laser light and the scattered light in the Raman process. The el-ph interaction is represented by the deformation-induced gauge field $\mathbf{A}^q = (A_x^q, A_y^q)$.¹⁵⁾ It can be shown that A_x^q and A_y^q are expressed in terms of a change of the nearest-neighbor hopping integral from an average value $-\gamma_0$, $\delta\gamma_{0,a}$, as¹⁶⁻¹⁸⁾

$$\begin{aligned} v_F A_x^q &= \delta\gamma_{0,1} - \frac{1}{2}(\delta\gamma_{0,2} + \delta\gamma_{0,3}), \\ v_F A_y^q &= \frac{\sqrt{3}}{2}(\delta\gamma_{0,2} - \delta\gamma_{0,3}). \end{aligned} \quad (3)$$

Here a ($= 1, 2, 3$) for $\delta\gamma_{0,a}$ denotes the direction of the bond (see the inset of Fig. 1), and $\delta\gamma_{0,a}$ is caused by atomic displacements by the Γ point optical phonon modes. Note that \mathbf{A}^q is uniform for the Γ point $\mathbf{q} = 0$ phonons, while \mathbf{A}^q depends on the position \mathbf{r} as $\mathbf{A}^q(\mathbf{r})$ for phonons with $\mathbf{q} \neq 0$.¹⁴⁾ Although an additional deformation-induced gauge field due to a local modulation of the hopping integral originating from a defect appears in a realistic situation, we ignore it in eq. (2) for simplicity.

3. Zigzag Edge

First, we calculate the matrix element relevant to the Raman intensity near the zigzag edge. The scattering or reflection of an electron at the zigzag edge is intravalley scattering,¹⁹⁾ and therefore we can consider the K and K' points separately. Let us consider the electrons near the K point. The Hamiltonian is given by

$$\hat{H}_K = v_F \boldsymbol{\sigma} \cdot (\hat{\mathbf{p}} + \mathbf{A}^q - e\mathbf{A}). \quad (4)$$

We specify the deformation-induced gauge field \mathbf{A}^q for the LO and TO modes near the zigzag edge. The vibrations of carbon atoms corresponding to the Γ point LO and TO modes are shown in Figs. 1(a) and 1(b). By assuming that the perturbation $\delta\gamma_{0,a}$ is proportional to the change in the bond length, we have $\delta\gamma_{0,1} = 0$ and $\delta\gamma_{0,2} = -\delta\gamma_{0,3}$ for the LO mode, while $\delta\gamma_{0,1} = -2\delta\gamma_{0,2}$ and $\delta\gamma_{0,2} = \delta\gamma_{0,3}$ for the TO mode. Using eq. (3), we see that \mathbf{A}^q for the LO mode is written as $\mathbf{A}_{LO}^q = (0, A_y^q)$ with $v_F A_y^q = \sqrt{3}\delta\gamma_{0,2}$, while \mathbf{A}^q for the TO mode is written as $\mathbf{A}_{TO}^q = (A_x^q, 0)$ with $v_F A_x^q = -3\delta\gamma_{0,2}$. Note that the direction of \mathbf{A}^q for the LO (TO) mode is perpendicular (parallel) to the zigzag edge. The direction of \mathbf{A}^q is perpendicular to the direction of atom displacement.^{9, 20)} Thus, the el-ph interaction in eq. (4), $H_{LO/TO}^{\text{zig}} \equiv v_F \boldsymbol{\sigma} \cdot \mathbf{A}_{LO/TO}^q$, is rewritten as

$$\begin{aligned} H_{LO}^{\text{zig}} &= v_F A_y^q \sigma_y, \\ H_{TO}^{\text{zig}} &= v_F A_x^q \sigma_x, \end{aligned} \quad (5)$$

for the LO and TO modes, respectively.

The el-ph matrix element is given as the expectation value of the el-ph interaction with respect to the energy eigenstate for the unperturbed Hamiltonian, $H_K^0 = v_F \boldsymbol{\sigma} \cdot \hat{\mathbf{p}}$. The energy eigenstate with wave vector \mathbf{k} in the conduction energy band is written in terms of the plane wave

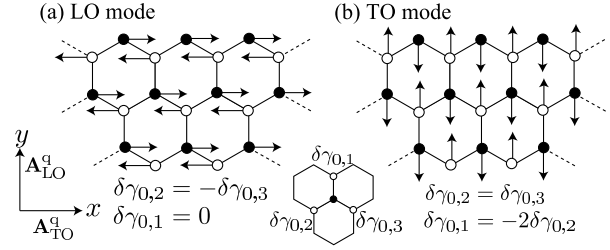


Fig. 1. The displacement vectors for the LO and TO modes are shown in (a) and (b), respectively. The displacement vectors of the LO (TO) mode are parallel (perpendicular) to the zigzag edge. The direction of the deformation-induced gauge field \mathbf{A}^q is perpendicular to the direction of atom displacement.

$e^{i\mathbf{k}\cdot\mathbf{r}}$ and the Bloch function $\Phi_{\mathbf{k}}^c$ as $\Phi_{\mathbf{k}}^c(\mathbf{r}) = N e^{i\mathbf{k}\cdot\mathbf{r}} \Phi_{\mathbf{k}}^c$, where N is a normalization constant satisfying $N^2 V = 1$, V is the area (volume) of the system, and

$$\Phi_{\mathbf{k}}^c \equiv \frac{1}{\sqrt{2}} \begin{pmatrix} 1 \\ e^{i\theta(\mathbf{k})} \end{pmatrix}. \quad (6)$$

Here $\theta(\mathbf{k})$ is the angle between the vector \mathbf{k} and the k_x -axis (see Fig. 2). The expectation values of σ_x , σ_y , and σ_z with respect to $\Phi_{\mathbf{k}}^c$ define the pseudospin. Since $\bar{\sigma}_x = \langle \Phi_{\mathbf{k}}^c | \sigma_x | \Phi_{\mathbf{k}}^c \rangle = \cos \theta(\mathbf{k})$, $\bar{\sigma}_y = \langle \Phi_{\mathbf{k}}^c | \sigma_y | \Phi_{\mathbf{k}}^c \rangle = \sin \theta(\mathbf{k})$, and $\bar{\sigma}_z = \langle \Phi_{\mathbf{k}}^c | \sigma_z | \Phi_{\mathbf{k}}^c \rangle = 0$, the direction of the pseudospin of $\Phi_{\mathbf{k}}^c$,

$$(\bar{\sigma}_x, \bar{\sigma}_y, \bar{\sigma}_z) = (\cos \theta(\mathbf{k}), \sin \theta(\mathbf{k}), 0), \quad (7)$$

is within the (k_x, k_y) plane and parallel to the vector \mathbf{k} (see Fig. 2). Owing to the presence of the zigzag edge parallel to the x -axis, the wave function near the zigzag edge is a standing wave given by a sum of the incident wave $\Phi_{\mathbf{k}}^c(\mathbf{r})$ and the reflected wave $\Phi_{\mathbf{k}'}^c(\mathbf{r})$ with $\mathbf{k}' \equiv (k_x, -k_y)$ as

$$\Psi_{\mathbf{k}}^c(\mathbf{r}) = \frac{1}{\sqrt{2}} (\Phi_{\mathbf{k}}^c(\mathbf{r}) + \Phi_{\mathbf{k}'}^c(\mathbf{r})). \quad (8)$$

Strictly speaking, it is necessary to add the relative phase between $\Phi_{\mathbf{k}}^c(\mathbf{r})$ and $\Phi_{\mathbf{k}'}^c(\mathbf{r})$ in order that $\Psi_{\mathbf{k}}^c(\mathbf{r})$ may satisfy the boundary condition for the zigzag edge. However, this phase gives no contribution to the matrix elements of interest in the present investigation, and therefore we omit it. Note that the normalization of eq. (8) is adopted for $k_y \neq 0$. Some complications arise when $k_y = 0$. For example, when $k_y = 0$ and $k_x < 0$, localized wave functions of edge states²¹⁾ should be used, which is explained in Appendix A.

The el-ph matrix element from a state in the conduction band to the same state is given as $\langle \Psi_{\mathbf{k}}^c | H_{LO/TO}^{\text{zig}} | \Psi_{\mathbf{k}}^c \rangle$. Using eqs. (5) and (8), the pseudospin, and $\theta(\mathbf{k}') = -\theta(\mathbf{k})$, we obtain

$$\langle \Psi_{\mathbf{k}}^c | H_{LO}^{\text{zig}} | \Psi_{\mathbf{k}}^c \rangle = 0, \quad (9)$$

$$\langle \Psi_{\mathbf{k}}^c | H_{TO}^{\text{zig}} | \Psi_{\mathbf{k}}^c \rangle = v_F A_x^q \cos \theta(\mathbf{k}). \quad (10)$$

This result shows that the Raman intensity of the LO mode is negligible compared with that of the TO mode at zigzag edges. For eq. (9), $\langle \Psi_{\mathbf{k}}^c | \sigma_y | \Psi_{\mathbf{k}}^c \rangle$ can be rewritten as a sum of two components, $\langle \Phi_{\mathbf{k}}^c | \sigma_y | \Phi_{\mathbf{k}}^c \rangle + \langle \Phi_{\mathbf{k}'}^c | \sigma_y | \Phi_{\mathbf{k}'}^c \rangle$, since cross terms such as $\langle \Phi_{\mathbf{k}}^c | \sigma_y | \Phi_{\mathbf{k}'}^c \rangle$ vanish. Because

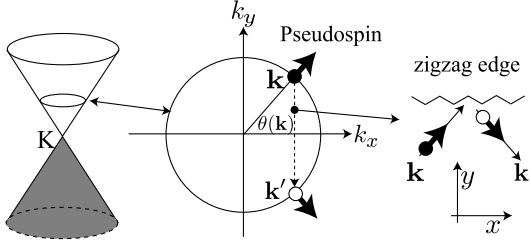


Fig. 2. The zigzag edge reflects the wave vector $\mathbf{k} = (k_x, k_y)$ to $\mathbf{k}' = (k_x, -k_y)$, and two wave functions $\Psi_{\mathbf{k}}^c(\mathbf{r})$ and $\Psi_{\mathbf{k}'}^c(\mathbf{r})$ form a standing wave. Note that the y -component of the pseudospin is flipped by the zigzag edge.

$\langle \Phi_{\mathbf{k}}^c | \sigma_y | \Phi_{\mathbf{k}}^c \rangle = \sin \theta(\mathbf{k})$ and $\langle \Phi_{\mathbf{k}'}^c | \sigma_y | \Phi_{\mathbf{k}'}^c \rangle = \sin \theta(\mathbf{k}') = -\sin \theta(\mathbf{k})$, the y -component of the pseudospin for the incident wave $\Phi_{\mathbf{k}}^c(\mathbf{r})$ is reflected as shown in Fig. 2. Thus, we have

$$\langle \Psi_{\mathbf{k}}^c | \sigma_y | \Psi_{\mathbf{k}}^c \rangle = 0, \quad (11)$$

due to the cancellation of the y -component of the pseudospin between the incident \mathbf{k} -state and the reflected \mathbf{k}' -state. Similarly, in eq. (10), $\langle \Psi_{\mathbf{k}}^c | \sigma_x | \Psi_{\mathbf{k}}^c \rangle$, is written as a sum of two components, $\langle \Phi_{\mathbf{k}}^c | \sigma_x | \Phi_{\mathbf{k}}^c \rangle + \langle \Phi_{\mathbf{k}'}^c | \sigma_x | \Phi_{\mathbf{k}'}^c \rangle$. Because $\langle \Phi_{\mathbf{k}}^c | \sigma_x | \Phi_{\mathbf{k}}^c \rangle = \cos \theta(\mathbf{k})$ and $\langle \Phi_{\mathbf{k}'}^c | \sigma_x | \Phi_{\mathbf{k}'}^c \rangle = \cos \theta(\mathbf{k}') = \cos \theta(\mathbf{k})$, we obtain eq. (10).

The Raman intensity depends on the polarization of the incident laser light²²⁾ and on that of the scattered light. The electron-light interaction is given by $H_K^{\text{em}} = -v_F e \boldsymbol{\sigma} \cdot \mathbf{A}$ in eq. (4). The optical absorption occurs with amplitude $M^{\text{opt}}(\mathbf{A}) = \langle \Psi_{\mathbf{k}}^c | H_K^{\text{em}} | \Psi_{\mathbf{k}}^v \rangle$, where $\Psi_{\mathbf{k}}^v(\mathbf{r})$ is the wave function in the valence energy band, which is related to $\Psi_{\mathbf{k}}^c(\mathbf{r})$ via $\Psi_{\mathbf{k}}^v(\mathbf{r}) = \sigma_z \Psi_{\mathbf{k}}^c(\mathbf{r})$. On the other hand, the optical emission occurs with amplitude $\langle \Psi_{\mathbf{k}}^v | H_K^{\text{em}} | \Psi_{\mathbf{k}}^c \rangle$, which is simply the complex conjugate of $M^{\text{opt}}(\mathbf{A})$. Thus, the polarization dependences of the incident and scattered light are the same. Here, let us examine the polarization dependence of the incident light. The direction of $\mathbf{A} = (A_x, A_y)$ corresponds to the direction of the polarization of the electric field. The polarization of the incident laser light should be perpendicular to the zigzag edge within a graphene plane, i.e., $\mathbf{A}_{\perp} = (0, A_y)$, in order to populate photoexcited electrons effectively. This argument follows from $M^{\text{opt}}(\mathbf{A}_{\perp}) = -iv_F e A_y \cos \theta(\mathbf{k})$ for $\mathbf{A}_{\perp} = (0, A_y)$, while $M^{\text{opt}}(\mathbf{A}_{\parallel}) = 0$ for $\mathbf{A}_{\parallel} = (A_x, 0)$ because

$$\begin{aligned} M^{\text{opt}}(\mathbf{A}_{\perp}) &\equiv -iv_F e A_y \langle \Psi_{\mathbf{k}}^c | \sigma_y | \Psi_{\mathbf{k}}^v \rangle \\ &= -iv_F e A_y \langle \Psi_{\mathbf{k}}^c | \sigma_y \sigma_z | \Psi_{\mathbf{k}}^c \rangle \\ &= -iv_F e A_y \langle \Psi_{\mathbf{k}}^c | \sigma_x | \Psi_{\mathbf{k}}^c \rangle \\ &= -iv_F e A_y \cos \theta(\mathbf{k}), \end{aligned} \quad (12)$$

and

$$\begin{aligned} M^{\text{opt}}(\mathbf{A}_{\parallel}) &\equiv -iv_F e A_x \langle \Psi_{\mathbf{k}}^c | \sigma_x | \Psi_{\mathbf{k}}^v \rangle \\ &= -iv_F e A_x \langle \Psi_{\mathbf{k}}^c | \sigma_x \sigma_z | \Psi_{\mathbf{k}}^c \rangle \\ &= iv_F e A_x \langle \Psi_{\mathbf{k}}^c | \sigma_y | \Psi_{\mathbf{k}}^c \rangle \\ &= 0. \end{aligned} \quad (13)$$

Here, we have used $|\Psi_{\mathbf{k}}^v\rangle = \sigma_z |\Psi_{\mathbf{k}}^c\rangle$, $\sigma_y \sigma_z = i\sigma_x$, $\sigma_x \sigma_z = -i\sigma_y$, and eq. (11). It is noteworthy that it is mainly the electrons near the k_x -axis [$\theta(\mathbf{k}) \approx 0$ or π] that can participate in the Raman process taking place near the zigzag edge since both the el-ph matrix element [eq. (10)] and the optical transition amplitude [eq. (12)] are proportional to $\cos \theta(\mathbf{k})$. Let us define the angle between the laser polarization and the zigzag edge as Θ (see the inset in Fig. 3), then $A_y = |\mathbf{A}| \sin \Theta$ and the Raman intensity is proportional to $|M^{\text{opt}}(\mathbf{A})|^2 \propto \sin^2 \Theta$. The Θ -dependence of the square of the optical transition amplitude is plotted as the dashed curve in Fig. 3.

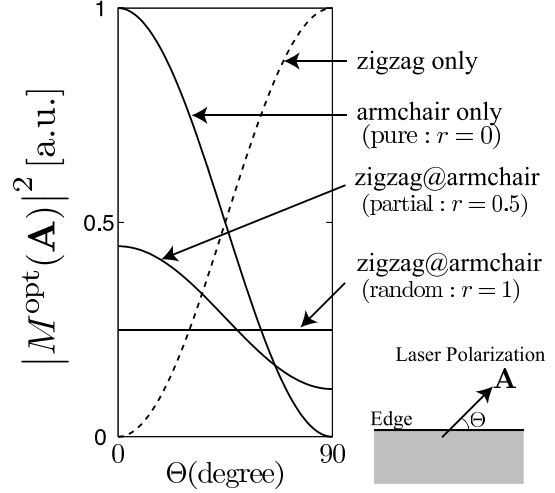


Fig. 3. The polarization dependence of the square of the optical transition amplitude ($|M^{\text{opt}}(\mathbf{A})|^2$) is plotted as a function of the angle of laser polarization (Θ) with respect to the orientation of the edge. For a pure zigzag (armchair) edge, the intensity is maximum when the laser polarization is perpendicular (parallel) to the edge. “zigzag@armchair” denotes the case when zigzag edges are introduced into part of a perfect armchair edge. We have used eq. (29) with $r = 0$ (armchair only), $r = 0.5$ (partial), and $r = 1$ (random: a mixture of zigzag and armchair edges).

The Kohn anomaly is relevant to the el-ph matrix element for electron-hole pair creation, i.e., $\langle \Psi_{\mathbf{k}}^c | H_{\text{LO/TO}}^{\text{zig}} | \Psi_{\mathbf{k}}^v \rangle$. Using $\Psi_{\mathbf{k}}^v(\mathbf{r}) = \sigma_z \Psi_{\mathbf{k}}^c(\mathbf{r})$, we rewrite the matrix element as $\langle \Psi_{\mathbf{k}}^c | H_{\text{LO/TO}}^{\text{zig}} \sigma_z | \Psi_{\mathbf{k}}^c \rangle$. From eq. (5), we have

$$\begin{aligned} H_{\text{LO}}^{\text{zig}} \sigma_z &= iv_F A_y^a \sigma_x, \\ H_{\text{TO}}^{\text{zig}} \sigma_z &= -iv_F A_x^a \sigma_y, \end{aligned} \quad (14)$$

where $\sigma_x \sigma_z = -i\sigma_y$ and $\sigma_y \sigma_z = i\sigma_x$ have been used. We have thus shown that $H_{\text{TO}}^{\text{zig}} \sigma_z$ is proportional to σ_y as well as that $H_{\text{LO}}^{\text{zig}}$ is proportional to σ_x . From eq. (11), we see that the TO mode is unable to transfer an electron in the valence band into the conduction band, that is, the TO mode does not decay into an electron-hole pair, and therefore the Kohn anomaly for the TO mode is negligible compared with that for the LO mode.

4. Armchair Edge

Next, we calculate the matrix element relevant to the Raman intensity near the armchair edge. Suppose that

the armchair edge is located along the y -axis, then the armchair edge reflects an electron with $\mathbf{k} = (k_x, k_y)$ near the K point into the state with $\mathbf{k}' = (k'_x, k'_y) = (-k_x, k_y)$ near the K' point, where \mathbf{k} and \mathbf{k}' are measured from the K and K' points, respectively. The negative sign in front of k_x for \mathbf{k}' is due to the momentum conservation. One may consider that an intervalley process is unconnected with the Γ point LO and TO phonons. Note, however, that we should consider the K and K' points simultaneously in the case of an armchair edge since the reflection of an electron by the armchair edge is an intervalley scattering process as shown in Fig. 4.

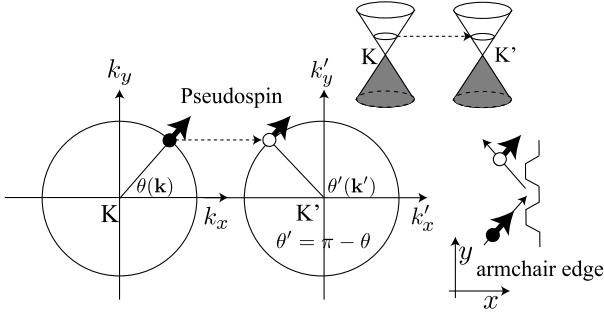


Fig. 4. The armchair edge reflects the wave vector $\mathbf{k} = (k_x, k_y)$ of one valley into $\mathbf{k}' = (-k_x, k_y)$ of another valley, and the two wave functions of the different valleys form a standing wave. The pseudospin is unchanged by the armchair edge. Note that the pseudospin for states near the K' point is not parallel to the vector \mathbf{k}' , while the pseudospin for states near the K point is parallel to the vector \mathbf{k} .

We specify the deformation-induced gauge field \mathbf{A}^q for the LO and TO modes near the armchair edge. The vibrations of carbon atoms for the Γ point LO and TO modes are shown in Fig. 5. We have $\delta\gamma_{0,1} = -2\delta\gamma_{0,2}$ and $\delta\gamma_{0,2} = \delta\gamma_{0,3}$ for the LO mode, while $\delta\gamma_{0,1} = 0$ and $\delta\gamma_{0,2} = -\delta\gamma_{0,3}$ for the TO mode. Using eq. (3), we see that \mathbf{A}^q for the LO mode is written as $\mathbf{A}_{\text{LO}}^q = (A_x^q, 0)$ with $v_F A_x^q = -3\delta\gamma_{0,2}$, while \mathbf{A}^q for the TO mode is written as $\mathbf{A}_{\text{TO}}^q = (0, A_y^q)$ with $v_F A_y^q = \sqrt{3}\delta\gamma_{0,2}$. Thus, from eq. (2), we see that the el-ph interaction

$$H_{\text{LO/TO}}^{\text{arm}} = v_F \begin{pmatrix} \boldsymbol{\sigma} \cdot \mathbf{A}_{\text{LO/TO}}^q & 0 \\ 0 & -\boldsymbol{\sigma}' \cdot \mathbf{A}_{\text{LO/TO}}^q \end{pmatrix} \quad (15)$$

is rewritten as

$$\begin{aligned} H_{\text{LO}}^{\text{arm}} &= v_F A_x^q \begin{pmatrix} \sigma_x & 0 \\ 0 & \sigma_x \end{pmatrix}, \\ H_{\text{TO}}^{\text{arm}} &= v_F A_y^q \begin{pmatrix} \sigma_y & 0 \\ 0 & -\sigma_y \end{pmatrix}, \end{aligned} \quad (16)$$

for the LO and TO modes, respectively.

The wave function is given by a sum of the plane wave at the K point and the reflected wave at the K' point as

$$\Psi_{\mathbf{k}}^c(\mathbf{r}) = \frac{e^{ik_y y}}{\sqrt{2}} \begin{pmatrix} \Phi_{\mathbf{k}}^c e^{ik_x x} \\ \Phi_{\mathbf{k}}^c e^{-ik_x x} \end{pmatrix}. \quad (17)$$

Note that the Bloch function is the same ($\Phi_{\mathbf{k}}^c$) for both the K and K' points. In fact, the Bloch function for a

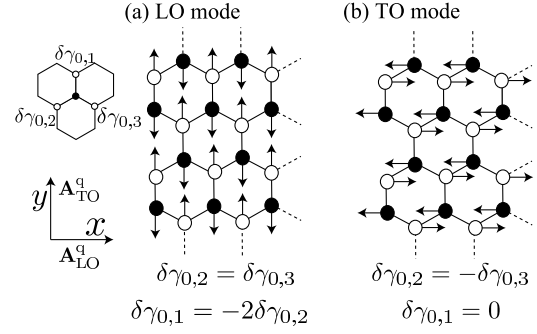


Fig. 5. The displacement vectors for the LO and TO modes are shown in (a) and (b), respectively. The displacement vectors of the LO (TO) mode are parallel (perpendicular) to the armchair edge. The direction of \mathbf{A}^q is perpendicular to the direction of atom displacement.

state near the K' point can be expressed as

$$\frac{1}{\sqrt{2}} \begin{pmatrix} 1 \\ -e^{-i\theta'(\mathbf{k}')} \end{pmatrix}, \quad (18)$$

where $\theta'(\mathbf{k}')$ is defined through $k'_x + ik'_y = |\mathbf{k}'|e^{i\theta'(\mathbf{k}'')}$. Since the armchair edge reflects the state with $\mathbf{k} = (k_x, k_y)$ into the state with $\mathbf{k}' = (-k_x, k_y)$, we have the relation $\theta'(\mathbf{k}') = \pi - \theta(\mathbf{k})$ (see Fig. 4). By substituting this into eq. (18), we see that the Bloch function of eq. (18) becomes $\Phi_{\mathbf{k}'}^c$ of eq. (6), which explains eq. (17). The pseudospin for the eigenstate near the K' point is given by $\langle \Phi_{\mathbf{k}'}^c | \sigma_x | \Phi_{\mathbf{k}'}^c \rangle = -\cos\theta'(\mathbf{k}')$ and $\langle \Phi_{\mathbf{k}'}^c | \sigma_y | \Phi_{\mathbf{k}'}^c \rangle = \sin\theta'(\mathbf{k}')$. Thus, the pseudospin for the K' point is not parallel to the vector \mathbf{k}' , as shown in Fig. 4, although the pseudospin for states near the K point is parallel to the vector \mathbf{k} . Using $\theta'(\mathbf{k}') = \pi - \theta(\mathbf{k})$, one can see that the pseudospin is preserved under the reflection at the armchair edge (see Fig. 4).

Using eqs. (16) and (17), it is straightforward to check that

$$\begin{aligned} \langle \Psi_{\mathbf{k}}^c | H_{\text{LO}}^{\text{arm}} | \Psi_{\mathbf{k}}^c \rangle &= v_F A_x^q \cos\theta(\mathbf{k}), \\ \langle \Psi_{\mathbf{k}}^c | H_{\text{TO}}^{\text{arm}} | \Psi_{\mathbf{k}}^c \rangle &= 0. \end{aligned} \quad (19)$$

This result shows that the Raman intensity of the TO mode is negligible compared with that of the LO mode. The absence of the Raman intensity of the TO mode results from the interference between two valleys, namely, the opposite signs in front of σ_y for the K and K' points of $H_{\text{TO}}^{\text{arm}}$ in eq. (16).

The interaction between the light and the electronic states is given by

$$H^{\text{em}}(\mathbf{A}) = -v_F e \begin{pmatrix} \boldsymbol{\sigma} \cdot \mathbf{A} & 0 \\ 0 & \boldsymbol{\sigma}' \cdot \mathbf{A} \end{pmatrix}, \quad (20)$$

from eq. (2). The optical absorption amplitude is given by $M^{\text{opt}}(\mathbf{A}) = \langle \Psi_{\mathbf{k}}^c | H^{\text{em}}(\mathbf{A}) | \Psi_{\mathbf{k}}^v \rangle$, where

$$\Psi_{\mathbf{k}}^v(\mathbf{r}) = \begin{pmatrix} \sigma_z & 0 \\ 0 & \sigma_z \end{pmatrix} \Psi_{\mathbf{k}}^c(\mathbf{r}). \quad (21)$$

If the polarization of the incident laser light is perpendicular to the armchair edge $\mathbf{A}_{\perp} = (A_x, 0)$, then $\langle \Psi_{\mathbf{k}}^c | H^{\text{em}}(\mathbf{A}_{\perp}) | \Psi_{\mathbf{k}}^v \rangle$ vanishes owing to the cancellation

between the K and K' points. The polarization of the incident laser should be parallel to the armchair edge, i.e., $\mathbf{A}_\parallel = (0, A_y)$, in order to populate photoexcited electrons effectively because $\langle \Psi_{\mathbf{k}}^c | H^{\text{em}}(\mathbf{A}_\parallel) | \Psi_{\mathbf{k}}^v \rangle = -iv_F e A_y \cos \theta(\mathbf{k})$. Note that it is mainly the electrons near the k_x -axis [$\theta(\mathbf{k}) \approx 0$ or π] that can participate the Raman process taking place near the armchair edge since both the el-ph matrix element [eq. (19)] and the optical transition amplitude are proportional to $\cos \theta(\mathbf{k})$. By defining the angle between the laser polarization and the armchair edge by Θ (see the inset in Fig. 3), we have $A_y = |\mathbf{A}| \cos \Theta$, and we see that the Raman intensity is proportional to $|M^{\text{opt}}(\mathbf{A})|^2 \propto \cos^2 \Theta$. The polarization dependence of the Raman intensity for the armchair edge is opposite that for the zigzag edge, as shown in Fig. 3, from which the orientation of the edge may be determined experimentally.

The el-ph matrix element for the Kohn anomaly is given by $\langle \Psi_{\mathbf{k}}^c | H_{\text{LO/TO}}^{\text{arm}} \sigma_z | \Psi_{\mathbf{k}}^c \rangle$. From eq. (16), we have

$$\begin{aligned} H_{\text{LO}}^{\text{arm}} \sigma_z &= -iv_F A_x^q \begin{pmatrix} \sigma_y & 0 \\ 0 & \sigma_y \end{pmatrix}, \\ H_{\text{TO}}^{\text{arm}} \sigma_z &= iv_F A_y^q \begin{pmatrix} \sigma_x & 0 \\ 0 & -\sigma_x \end{pmatrix}. \end{aligned} \quad (22)$$

It has thus been shown that the TO mode does not undergo a Kohn anomaly because the matrix element vanishes owing to the sign difference between the K and K' points with respect to σ_x .

5. Energy Difference Between LO and TO Modes

In this section we calculate the energy difference between the LO and TO modes. The renormalized phonon energy is written as a sum of the unrenormalized energy $\hbar\omega$ and the self-energy. Since the TO mode does not undergo a Kohn anomaly, the self-energy of the TO mode vanishes. Thus, the energy difference between the LO and TO modes is the self-energy of the LO mode, which is given by time-dependent second-order perturbation theory as

$$\begin{aligned} \Pi(\omega, E_F) &= 2 \sum_{\mathbf{k}} \left(\frac{|\langle \Psi_{\mathbf{k}}^c | H_{\text{LO}}^{\text{arm}} | \Psi_{\mathbf{k}}^v \rangle|^2}{\hbar\omega - E_{\mathbf{k}}^{\text{eh}} + i\delta} - \frac{|\langle \Psi_{\mathbf{k}}^c | H_{\text{LO}}^{\text{arm}} | \Psi_{\mathbf{k}}^v \rangle|^2}{\hbar\omega + E_{\mathbf{k}}^{\text{eh}} + i\delta} \right) \\ &\quad \times (f_h - f_e), \end{aligned} \quad (23)$$

where the factor of 2 originates from the spin degeneracy, $f_{e,h} = (1 + \exp((E^{e,h} - E_F)/k_B T))^{-1}$ is the Fermi distribution function, E_F is the Fermi energy, δ is a positive infinitesimal, E^e (E^h) is the energy of an electron (a hole), and $E_{\mathbf{k}}^{\text{eh}} \equiv E_{\mathbf{k}}^e - E_{\mathbf{k}}^h = 2\hbar v_F |\mathbf{k}|$ (≥ 0) is the energy of an electron-hole pair. Note that the summation index $\sum_{\mathbf{k}}$ in eq. (23) is not restricted to only interband ($E^{\text{eh}} \neq 0$) processes but also includes intraband ($E^{\text{eh}} = 0$) processes. Thus, the self-energy can be decomposed into two parts, $\Pi(\omega, E_F) = \Pi^{\text{inter}}(\omega, E_F) + \Pi^{\text{intra}}(\omega, E_F)$, where $\Pi^{\text{inter}}(\omega, E_F)$ includes only interband electron-hole pair creation processes satisfying $E^{\text{eh}} \neq 0$.

In the adiabatic limit, i.e., when $\omega = 0$ and $\delta = 0$ in eq. (23), by substituting eq. (19) into eq. (23), it is

straightforward to show that, at $T = 0$,

$$\begin{aligned} \Pi^{\text{intra}}(0, E_F) &= -\frac{V}{\pi} \left(\frac{A_x^q}{\hbar} \right)^2 |E_F|, \\ \Pi^{\text{inter}}(0, E_F) &= -\frac{V}{\pi} \left(\frac{A_x^q}{\hbar} \right)^2 (E_c - |E_F|), \end{aligned} \quad (24)$$

where E_c is a cutoff energy. Note that $\Pi^{\text{intra}}(0, E_F)$ does not vanish because $(f_h - f_e)/E_{\mathbf{k}}^{\text{eh}} \neq 0$ in the limit of $E_{\mathbf{k}}^{\text{eh}} \rightarrow 0$, while in the nonadiabatic case, $\Pi^{\text{intra}}(\omega, E_F)$ vanishes since $(f_h - f_e)/\hbar\omega = 0$ in this limit. It is only the interband process that contributes to the self-energy in the nonadiabatic case. Lazzeri and Mauri¹¹⁾ pointed out that $\Pi(0, E_F)$ does not depend on E_F in the adiabatic limit owing to the cancellation between $\Pi^{\text{intra}}(0, E_F)$ and $\Pi^{\text{inter}}(0, E_F)$. This shows that the adiabatic approximation is not appropriate for discussing the E_F dependence of the self-energy. In the nonadiabatic case, at $T = 0$, it is a straightforward calculation to obtain (see Appendix B for derivation)

$$\begin{aligned} \text{Re} [\Pi(\omega, E_F)] &= \\ &= -\frac{V}{\pi} \left(\frac{A_x^q}{\hbar} \right)^2 \left[E_c - |E_F| - \frac{\hbar\omega}{4} \ln \left| \frac{|E_F| - \frac{\hbar\omega}{2}}{|E_F| + \frac{\hbar\omega}{2}} \right| \right]. \end{aligned} \quad (25)$$

The Fermi energy dependence is given by the last two terms.^{10,11)} The first term is linear with respect to E_F and the second term produces a singularity at $E_F = \pm \hbar\omega/2$. These terms express the nonadiabatic effects.²³⁾ Recently, Saitta *et al.*²⁴⁾ have pointed out that large nonadiabatic effects are found to be more ubiquitous in layered metals such as CaC₆ and MgB₂.

For the case of $E_F = 0$, eq. (25) becomes

$$\text{Re} [\Pi(\omega, 0)] = -\frac{V}{\pi} \left(\frac{A_x^q}{\hbar} \right)^2 E_c. \quad (26)$$

The self-energy depends on the cutoff energy E_c . The value of E_c cannot be determined within the effective-mass model. We assume that E_c is of the order of half of the π bandwidth (10 eV); see §7 for a detailed discussion of the value of E_c . Using the harmonic approximation for the displacement of the carbon atoms,²⁵⁾ we obtain $\sqrt{N_u} |A_x^q/\hbar| \approx 2 \times 10^{-2} \text{\AA}^{-1}$ (see Appendix B), where N_u denotes the number of hexagonal unit cells. Since V can be written as $N_u S$ where S is the area of a hexagonal unit cell, we obtain $\text{Re} [\Pi(\omega, 0)] \approx -6 \text{ meV}$. Thus, the difference in the Raman shift between the (Raman active) TO mode near the zigzag edge and the (Raman active) LO mode near the armchair edge is approximately 50 cm^{-1} . In a realistic system, the actual magnitude of the self-energy may be much smaller than this value. For example, a typical edge is a mixture of zigzag and armchair edges, for which the energy difference between the LO and TO modes is lower.

Here, let us introduce zigzag edges into part of a perfect armchair edge at $x = 0$ and examine the effect of the randomness of the edge shape on the Raman intensity and phonon self-energies. Then the standing wave

near the rough edge is approximated by

$$\Psi_{\mathbf{k}}^c(\mathbf{r}) = e^{i\mathbf{k}\cdot\mathbf{r}} \begin{pmatrix} \Phi_{\mathbf{k}}^c \\ 0 \end{pmatrix} + ae^{i\mathbf{k}'\cdot\mathbf{r}} \begin{pmatrix} 0 \\ \Phi_{\mathbf{k}}^c \end{pmatrix} + ze^{i\mathbf{k}'\cdot\mathbf{r}} \begin{pmatrix} \Phi_{\mathbf{k}'}^c \\ 0 \end{pmatrix}, \quad (27)$$

where $\mathbf{k}' = (-k_x, k_y)$ and $|a|^2 + |z|^2 = 1$. The wave function $\Psi_{\mathbf{k}}^c(\mathbf{r})$ reproduces eq. (17) for the case when $(a, z) = (1, 0)$. Note that $|z|^2/|a|^2$ ($\equiv r \leq 1$) can be considered phenomenologically as the ratio of the number of zigzag edges to that of armchair edges in the rough edge, and $r = 1$ ($(|a|, |z|) = (1/\sqrt{2}, 1/\sqrt{2})$) represents the case that armchair and zigzag edges are equally distributed along the y -axis. It is a straightforward calculation to obtain

$$\begin{aligned} \langle \Psi_{\mathbf{k}}^c | H_{\text{LO}}^{\text{arm}} | \Psi_{\mathbf{k}}^c \rangle &= v_F A_x^q \cos \theta(\mathbf{k}) \frac{1 + |a|^2 - |z|^2}{1 + |a|^2 + |z|^2}, \\ \langle \Psi_{\mathbf{k}}^c | H_{\text{TO}}^{\text{arm}} | \Psi_{\mathbf{k}}^c \rangle &= v_F A_y^q \sin \theta(\mathbf{k}) \frac{1 - |a|^2 + |z|^2}{1 + |a|^2 + |z|^2}. \end{aligned} \quad (28)$$

These matrix elements show that the self-energy for the LO mode becomes $\text{Re}[\Pi(\omega, 0)]/4$ for the case of $r = 1$. On the other hand, the self-energy of the TO mode, which is zero for the case of $r = 0$, becomes $\text{Re}[\Pi(\omega, 0)]/4$ for the case of $r = 1$. The differences in the Kohn anomalies for the LO and TO modes disappear for the case of $r = 1$. Moreover, the Raman intensity of the TO mode increases, while the Raman intensity of the LO mode decreases. As a result, the G band exhibits a single peak. The intensity of the G band is given as the sum of the LO and TO modes. Since the intensity of each mode is four times smaller than that of the LO mode near the pure armchair edge, the total intensity of the G band should be two times smaller than the Raman intensity near the pure armchair edge. Note that for a general value of (a, z) , the energy difference between the LO and TO modes is given by $(|a|^2 - |z|^2)\text{Re}[\Pi(\omega, 0)]$. It is also a straightforward calculation to obtain the polarization dependence of the optical transition amplitude,

$$|M^{\text{opt}}(\mathbf{A})|^2 \propto \frac{\cos^2 \Theta}{(1+r)^2} + \frac{r^2 \sin^2 \Theta}{(1+r)^2}. \quad (29)$$

This dependence is plotted for two cases, $r = 1$ and $r = 0.5$, in Fig. 3.

6. Bulk and Edge

In the case of an infinite periodic graphene system without an edge, the self-energies of the LO and TO modes are the same and given by $\text{Re}[\Pi(\omega, E_F)]$ in eq. (25). Moreover, no asymmetry between the LO and TO modes in the Raman intensity is expected. The reason why the LO and TO modes do not exhibit any difference in Raman spectra is that graphene is a homo-polar crystal with two atoms per unit cell, and hence there is no polar mode, similar to the case of Si. Thus, the LO and TO modes are degenerate and contribute equally to the single peak of the G band (see ‘‘Periodic’’ in Fig. 6). Note that a slight change in the spring force constant due to a uniaxial strain applied to a graphene sample can resolve the degeneracy between the LO and TO modes. In this case, the unrenormalized energy $\hbar\omega$ for the LO mode

is not identical to that for the TO mode. However, even for this case, we can expect that the self-energies and Raman intensities for the LO and TO modes are similar to each other. Thus, we can see two peaks for the LO and TO modes with similar intensity, as was observed by Mohiuddin *et al.*²⁶⁾

Since an actual sample is always surrounded by an edge, it is interesting to consider whether or not the interior of a graphene sample can be considered as an infinite periodic graphene system without the edge. If the wave function in the interior region is given by a superposition of the incident and reflected states, then it is reasonable to assume that the wave function is approximated by eq. (27) with $(|a|, |z|) = (1/\sqrt{2}, 1/\sqrt{2})$, since it is probable that the edge is a random mixture of zigzag and armchair edges. The peak positions of the LO and TO modes in the Raman shift are indicated by ‘‘Random’’ in Fig. 6. We speculate that the peak position for an actual sample appears between the peaks labeled ‘‘Periodic’’ and ‘‘Random’’. An estimation of the effective distance from the edge at which the effect of interference on the pseudospin discussed so far can survive will be a subject of further investigation.

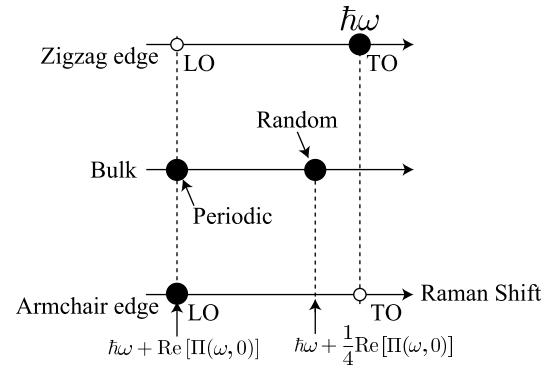


Fig. 6. The horizontal lines indicate the Raman shift for the case of $E_F = 0$. (top and bottom lines) The Raman peak taken near the zigzag (armchair) edge appears only for the TO (LO) mode indicated by the solid circle. The peak for the TO mode does not accompany the broadening because the TO mode decouples from the electron-hole pairs. (middle line) The Raman peak appears at $\hbar\omega + \text{Re}[\Pi(\omega, 0)]$ in the case of an infinite periodic graphene system without an edge (‘‘Periodic’’). If the effect of the electron reflection at the edge survives in the interior of a graphene sample (‘‘Random’’), the Raman peak is expected to appear at $\hbar\omega + \text{Re}[\Pi(\omega, 0)]/4$.

7. Discussion and Conclusions

Here, we discuss the relationship between our result and experimental results. Cançado *et al.* observed that the Raman intensity of the G band for a nanoribbon has a strong dependence on the incident light polarization.²⁷⁾ They showed that the Raman intensity is maximum when the polarization is parallel to the edge of a nanoribbon. Their result is consistent with our result for the armchair edge, but not consistent with our result for the zigzag edge. We speculate that the sample used in their experiment is similar to a nanoribbon with an arm-

chair edge. This speculation is reasonable because armchair edges are more frequently observed in experiments than zigzag edges.²⁸⁾ Casiraghi *et al.* performed Raman spectroscopy on graphene edges and observed a small redshift of the G peak near the edge accompanied by a decrease in the linewidth of the G peak.²⁹⁾ This behavior of the G peak is consistent with that of the zigzag edge since it is only the TO mode without broadening (which is related to the imaginary part of the self-energy) that can be Raman active.

The cutoff energy E_c appearing in eq. (26) may be determined from a tight-binding lattice model. For periodic graphene, by taking into account the contribution of all the possible electron-hole intermediate states in the Brillouin zone, we can have $E_c \approx 7\gamma_0$ (20 eV), which is larger than the value adopted in eq. (26). The value of E_c for a graphene sample with an edge may be different from that for a periodic graphene sample without an edge. In fact, for a nanoribbon, a tight-binding calculation²⁵⁾ shows that the energy difference between the LO and TO modes is approximately 30 cm^{-1} , which corresponds to $E_c \approx 6 \text{ eV}$. Thus the value of E_c depends on the geometry of the system. Since we have considered a large graphene sample with an edge, we assumed that an appropriate value of E_c is between 6 and 20 eV, and we chose 10 eV, which is of the order of half of the π bandwidth. Because E_c is not an experimentally controllable parameter, we consider that, in order to verify our results, it is essential to observe the E_F dependence of the G band spectra near the edge.

In conclusion, the el-ph matrix elements for the Raman intensity and Kohn anomaly near the edge of graphene were derived by adiabatic calculation, and then perturbation treatment was applied to the nonadiabatic parts of the phonon self-energies. The zigzag edge causes intravalley scattering and the y -component of the pseudospin vanishes $\langle \sigma_y \rangle = 0$ for the standing wave. The Raman intensity of the LO mode and the Kohn anomaly of the TO mode are negligible owing to $\langle \sigma_y \rangle = 0$. On the other hand, the armchair edge causes intervalley scattering and the pseudospin does not change its direction. However, owing to the interference between two valleys originating from the el-ph interaction, the Raman intensity and Kohn anomaly are negligible only for the TO mode. The Raman intensity is enhanced when the polarization of the incident laser is parallel (perpendicular) to the armchair (zigzag) edge. The difference in the behavior of the pseudospin with respect to the zigzag and armchair edges is the origin of the asymmetry between the LO and TO modes. Our results are summarized in Table I.

Acknowledgments

K. S. would like to thank T. Osada (Institute for Solid State Physics, University of Tokyo) for a useful comment on the pseudospin for states near the K' point. R. S. acknowledges a MEXT Grant (No. 20241023). This work was supported by a Grant-in-Aid for Specially Promoted Research (No. 20001006) from MEXT.

Table I. Dependences of the Raman intensities and Kohn anomalies on the Γ point optical phonon modes. The symbols \circ and \times for Raman intensity and the Kohn anomaly represent ‘occurrence’ and ‘absence’, respectively. There is asymmetry between the Raman intensity and Kohn anomaly, that is, the Kohn anomaly occurs only for the LO mode, while the mode with a strong Raman intensity changes according to the edge shape. Raman intensity is enhanced when the polarization of the incident laser light is parallel (LO) to the armchair edge or when it is perpendicular (TO) to the zigzag edge.

Position	Mode	Raman	Kohn	Polarization
zigzag	LO	\times	\circ	\times
	TO	\circ	\times	\circ
armchair	LO	\circ	\circ	\circ
	TO	\times	\times	\times
bulk	LO	\circ	\circ	\circ
	TO	\circ	\circ	\circ

Appendix A: Correction of Edge States to eq. (10)

Here, we exactly calculate the x -component of the pseudospin, $\langle \Psi_{\mathbf{k}}^c | \sigma_x | \Psi_{\mathbf{k}}^c \rangle$, with $k_y = 0$. When $k_y \rightarrow 0$, we have

$$\langle \Psi_{\mathbf{k}}^c | \sigma_x | \Psi_{\mathbf{k}}^c \rangle = \cos \theta(\mathbf{k}). \quad (\text{A}\cdot 1)$$

It should be noted that this expression holds for extended states. The states with $k_y = 0$ are divided into two states, extended states and edge states,²¹⁾ depending on the sign of k_x .³⁰⁾ For the K point, the edge states satisfy $k_x < 0$, while the extended states satisfy $k_x > 0$. Since the edge states are pseudospin polarization states, that is, they are eigenstates of σ_z , then the matrix element of σ_x with respect to the edge states vanishes. Thus, the exact form is given by

$$\langle \Psi_{\mathbf{k}}^c | \sigma_x | \Psi_{\mathbf{k}}^c \rangle = \begin{cases} \cos \theta(\mathbf{k}) & (k_y \neq 0), \\ \text{sign}(k_x) \cos \theta(\mathbf{k}) & (k_y = 0), \end{cases} \quad (\text{A}\cdot 2)$$

where $\text{sign}(k_x) = 1$ when $k_x > 0$ and zero otherwise. By neglecting this complication, we obtain eq. (10).

Appendix B: Derivation of eq. (25)

In this section, we derive eq. (25).

First, using eqs. (17) and (22), we obtain

$$\langle \Psi_{\mathbf{k}}^c | H_{\text{LO}}^{\text{arm}} | \Psi_{\mathbf{k}}^v \rangle = -iv_F A_x^q \sin \theta(\mathbf{k}). \quad (\text{B}\cdot 1)$$

Next, we consider the real part of the self-energy by setting $\delta = 0$ in eq. (23). At zero temperature, we can set $f_h - f_e = 1$ for $E_{\mathbf{k}}^e \geq |E_F|$, otherwise $f_h - f_e = 0$. Then, the self-energy of the LO mode is written as

$$\text{Re} [\Pi(\omega, E_F)] = 2(v_F A_x^q)^2 \sum_{\mathbf{k}}' \left\{ \frac{\sin^2 \theta(\mathbf{k})}{\hbar\omega - E_{\mathbf{k}}^e} - \frac{\sin^2 \theta(\mathbf{k})}{\hbar\omega + E_{\mathbf{k}}^{\text{eh}}} \right\}, \quad (\text{B}\cdot 2)$$

where \sum' indicates that the summation is taken over states satisfying $E_{\mathbf{k}}^e \geq |E_F|$. Since the y -axis (x -axis) is parallel (perpendicular) to the armchair edge, we use a periodic boundary condition for k_y and an open boundary condition for k_x . Then we have $k_y = 2\pi n_y / L_y$ and $k_x = \pi n_x / L_x$. The summation over possible electron-hole

pairs can be rewritten as

$$\sum_{\mathbf{k}} = 2 \left[\frac{V}{2\pi^2} \int_0^{k_c} dk_x \int_{-k_c}^{k_c} dk_y \right], \quad (\text{B}\cdot\text{3})$$

where $V \equiv L_x L_y$, k_c is the cutoff momentum, and the factor of 2 originates from the degeneracy with respect to the K and K' points. Substituting eq. (B·3) into eq. (B·2), we have

$$\begin{aligned} \text{Re} [\Pi(\omega, E_F)] &= \frac{2V}{\pi^2} \left(\frac{A_x^q}{\hbar} \right)^2 \int_{-\pi/2}^{\pi/2} \sin^2 \theta d\theta \\ &\times \int_{|E_F|}^{E_c} E dE \left\{ \frac{1}{\hbar\omega - 2E} - \frac{1}{\hbar\omega + 2E} \right\}, \end{aligned} \quad (\text{B}\cdot\text{4})$$

where we have changed the integration variables from (k_x, k_y) to (E, k) by using $k_x = k \cos \theta$, $k_y = k \sin \theta$, and $E = \hbar v_F k$. Using $\int_{-\pi/2}^{\pi/2} \sin^2 \theta d\theta = \pi/2$ and $\int x/(x+a) dx = x - a \ln|x+a|$, we obtain eq. (25) when $E_c \gg \hbar\omega$.

To calculate A_x^q , we have used $A_x^q \equiv g_{\text{off}} u(\omega)/a_{\text{cc}}$ where $a_{\text{cc}} = 1.42 \text{ \AA}$. Here g_{off} is the off-site el-ph matrix element and $u(\omega)$ is the amplitude of the phonon mode. We adopt $g_{\text{off}} = 6.4 \text{ eV}$.³¹⁾ A similar value is obtained by a first-principles calculation with the local density approximation.³²⁾ We use a harmonic oscillator model which gives $u(\omega) = \sqrt{\hbar/2M_c N_u \omega}$, where M_c is the mass of a carbon atom. Using $\hbar\omega = 0.2 \text{ eV}$, we obtain $\sqrt{N_u} |A_x^q/\hbar| \approx 2 \times 10^{-2} \text{ \AA}^{-1}$.

- 1) K. S. Novoselov, A. K. Geim, S. V. Morozov, D. Jiang, M. I. Katsnelson, I. V. Grigorieva, S. V. Dubonos, and A. A. Firsov, *Nature* **438**, 197 (2005).
- 2) Y. Zhang, Y.-W. Tan, H. Stormer, and P. Kim, *Nature* **438**, 201 (2005).
- 3) A. Bostwick, T. Ohta, T. Seyller, K. Horn, and E. Rotenberg, *Nature Physics* **3**, 36 (2007).
- 4) A. C. Ferrari, J. C. Meyer, V. Scardaci, C. Casiraghi, M. Lazzeri, F. Mauri, S. Piscanec, D. Jiang, K. S. Novoselov, S. Roth, and A. K. Geim, *Phys. Rev. Lett.* **97**, 187401 (2006).
- 5) J. Yan, Y. Zhang, P. Kim, and A. Pinczuk, *Phys. Rev. Lett.* **98**, 166802 (2007).
- 6) D. V. Kosynkin, A. L. Higginbotham, A. Sinitskii, J. R. Lomeda, A. Dimiev, B. K. Price, and J. M. Tour, *Nature* **458**, 872 (2009).
- 7) L. Jiao, L. Zhang, X. Wang, G. Diankov, and H. Dai, *Nature* **458**, 877 (2009).
- 8) W. Kohn, *Phys. Rev. Lett.* **2**, 393 (1959).

- 9) O. Dubay, G. Kresse, and H. Kuzmany, *Phys. Rev. Lett.* **88**, 235506 (2002).
- 10) T. Ando, *J. Phys. Soc. Jpn.* **75**, 124701 (2006).
- 11) M. Lazzeri and F. Mauri, *Phys. Rev. Lett.* **97**, 266407 (2006).
- 12) S. Piscanec, M. Lazzeri, F. Mauri, A. C. Ferrari, and J. Robertson, *Phys. Rev. Lett.* **93**, 185503 (2004).
- 13) H. Farhat, H. Son, G. G. Samsonidze, S. Reich, M. S. Dresselhaus, and J. Kong, *Phys. Rev. Lett.* **99**, 145506 (2007).
- 14) K. Sasaki, R. Saito, G. Dresselhaus, M. S. Dresselhaus, H. Farhat, and J. Kong, *Phys. Rev. B* **77**, 245441 (2008).
- 15) K. Sasaki and R. Saito, *Prog. Theor. Phys. Suppl.* **176**, 253 (2008).
- 16) C. L. Kane and E. J. Mele, *Phys. Rev. Lett.* **78**, 1932 (1997).
- 17) K. Sasaki, Y. Kawazoe, and R. Saito, *Prog. Theor. Phys.* **113**, 463 (2005).
- 18) M. Katsnelson and A. Geim, *Phil. Trans. R. Soc. A* **366**, 195 (2008).
- 19) M. A. Pimenta, G. Dresselhaus, M. S. Dresselhaus, L. G. Cançado, A. Jorio, and R. Saito, *Phys. Chem. Chem. Phys.* **9**, 1276 (2007).
- 20) K. Ishikawa and T. Ando, *J. Phys. Soc. Jpn.* **75**, 084713 (2006).
- 21) M. Fujita, K. Wakabayashi, K. Nakada, and K. Kusakabe, *J. Phys. Soc. Jpn.* **65**, 1920 (1996).
- 22) A. Grüneis, R. Saito, G. G. Samsonidze, T. Kimura, M. A. Pimenta, A. Jorio, A. G. S. Filho, G. Dresselhaus, and M. S. Dresselhaus, *Phys. Rev. B* **67**, 165402 (2003).
- 23) S. Pisana, M. Lazzeri, C. Casiraghi, K. S. Novoselov, A. K. Geim, A. C. Ferrari, and F. Mauri, *Nature Materials* **6**, 198 (2007).
- 24) A. M. Saitta, M. Lazzeri, M. Calandra, and F. Mauri, *Phys. Rev. Lett.* **100**, 226401 (2008).
- 25) K. Sasaki, M. Yamamoto, S. Murakami, R. Saito, M. Dresselhaus, K. Takai, T. Mori, T. Enoki, and K. Wakabayashi, *Phys. Rev. B* **80**, 155450 (2009).
- 26) T. M. G. Mohiuddin, A. Lombardo, R. R. Nair, A. Bonetti, G. Savini, R. Jalil, N. Bonini, D. M. Basko, C. Galotias, N. Marzari, K. S. Novoselov, A. K. Geim, and A. C. Ferrari, *Phys. Rev. B* **79**, 205433 (2009).
- 27) L. G. Cançado, M. A. Pimenta, B. R. A. Neves, G. Medeiros-Ribeiro, T. Enoki, Y. Kobayashi, K. Takai, K.-i. Fukui, M. S. Dresselhaus, R. Saito, and A. Jorio, *Phys. Rev. Lett.* **93**, 47403 (2004).
- 28) Y. Kobayashi, K. Fukui, T. Enoki, K. Kusakabe, and Y. Kaburagi, *Phys. Rev. B* **71**, 193406 (2005).
- 29) C. Casiraghi, A. Hartschuh, H. Qian, S. Piscanec, C. Georgi, A. Fasoli, K. S. Novoselov, D. M. Basko, and A. C. Ferrari, *Nano Letters* **9**, 1433 (2009).
- 30) K. Sasaki, S. Murakami, and R. Saito, *J. Phys. Soc. Jpn.* **75**, 074713 (2006).
- 31) J. Jiang, R. Saito, G. G. Samsonidze, S. G. Chou, A. Jorio, G. Dresselhaus, and M. S. Dresselhaus, *Phys. Rev. B* **72**, 235408 (2005).
- 32) D. Porezag, T. Frauenheim, T. Köhler, G. Seifert, and R. Kaschner, *Phys. Rev. B* **51**, 12947 (1995).